

# Formation of binary liquid crystal mixtures from a thermal cyclization process

Cécile Canlet,<sup>a</sup> Masood A. Khan,<sup>a</sup> Bing M. Fung,<sup>a</sup> Frédéric Roussel,<sup>b</sup> Patrick Judeinstein<sup>c</sup> and Jean-Pierre Bayle<sup>\*c</sup>

<sup>a</sup> Department of Chemistry and Biochemistry, University of Oklahoma, Norman, Oklahoma, 73019-0370, USA

<sup>b</sup> Laboratoire de Dynamique et Structure des Matériaux Moléculaires, Université du Littoral (CNRS URA 801), MREID, 59140 Dunkerque, France

<sup>c</sup> Laboratoire de Chimie Structurale Organique (CNRS URA 1384), Université Paris XI, 91405 Orsay cedex, France. E-mail: jpbayle@icmo.u-psud.fr

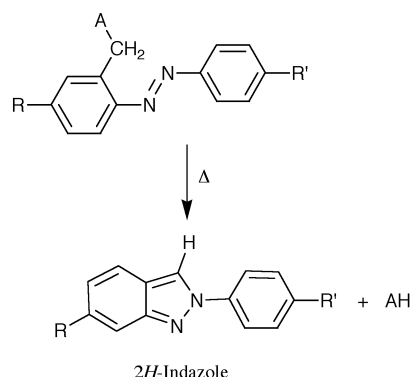
Received (in Montpellier, France) 2nd September 1999, Accepted 18th October 1999

An unusual process, the change of an isotropic phase into a nematic phase at a constant temperature, is reported. The conversion is the result of the thermal cyclization of a single compound, which is either isotropic or nematic, to form two compounds, both of which are enantiotropic liquid crystals. The starting material is a class of compounds having a diazo link between two *para*-substituted phenyl rings and a 4-*n*-alkoxybenzoyloxymethylene lateral group in the *ortho* position with respect to the diazo link. The DSC curves and optical microscopy show that, after melting, the compound undergoes an exothermic reaction to form a mixture that has liquid crystalline properties over a wide temperature range. The mixture is composed of two mesogenic compounds: a disubstituted 2*H*-indazole and a 4-*n*-alkoxybenzoic acid. The liquid crystalline properties are reproducible in further heating-cooling cycles. The time-dependent <sup>13</sup>C NMR spectra at a constant temperature slightly above the melting temperature indicate that a small extent of reaction is sufficient to induce liquid crystalline properties in the melt. Optical measurement of the appearance of the nematic phase at different constant temperatures gives the activation energy of the reaction as  $71.5 \pm 0.8$  and  $81.8 \pm 1.2$  kJ mol<sup>-1</sup> for the two series of compounds studied. The X-ray structure of a parent compound shows the coplanarity and the rigidity of the central core containing the 2*H*-indazole fragment and the attached aromatic ring. This central core is slightly bent with an angle of 157° between the terminal bonds.

## Introduction

It is well-known that phenyldiazenes having a methyl or an activated methylene group in the *ortho* position to the diazo linkage can undergo a unimolecular reaction to yield 2*H*-indazoles, as shown in Scheme 1.<sup>1-6</sup>

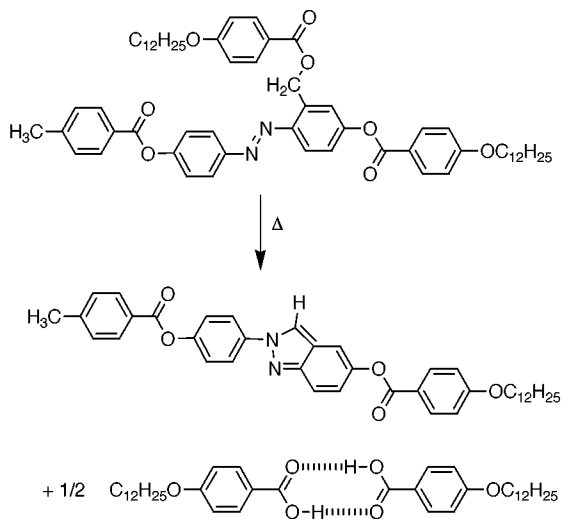
In the course of the reaction, the red color induced by the diazo linkage disappears, turning into a white mixture. The activated methylene can be any CH<sub>2</sub> group bearing a leaving group, such as a hydroxy group (A = OH), an alkoxy group (A = OR)<sup>7-9</sup> or an *N,N*-dialkylated methylene amine group (A = NR<sub>2</sub>).<sup>10</sup> Noting that the 2*H*-indazole fragment can act as



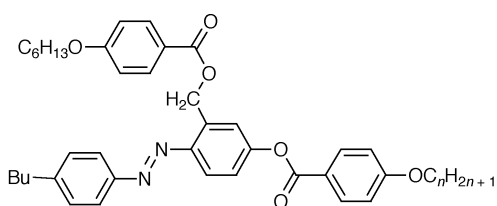
Scheme 1

an interesting rigid component to build new mesogenic structures, we have recently studied liquid crystal systems that can undergo this type of thermal cyclization.<sup>10</sup> The compounds investigated had four aromatic rings in the main core and a lateral *N,N*-dialkylated methylene amine fragment on one of the inner aromatic rings. During the cyclization process, the core containing the 2*H*-indazole fragment was produced, leading to a mixture having interesting liquid crystalline properties. The intramolecular reaction was quite clean as evidenced by NMR, DSC and TGA.<sup>10</sup> Unfortunately, one of the products formed in the reaction was an *N,N*-dialkylated amine, which strongly depressed the transition temperatures. Therefore, it is desirable that the leaving molecule has mesogenic properties. The simplest choice is to use 4-*n*-alkoxybenzoic acids because it is well-known that these acids form dimers and have noticeable nematogen properties.<sup>11</sup> Thus, we can expect to obtain, after the cyclization process, a nice nematic mixture composed of a nematogen containing the 2*H*-indazole fragment and the 4-*n*-alkoxybenzoic acid (Scheme 2).

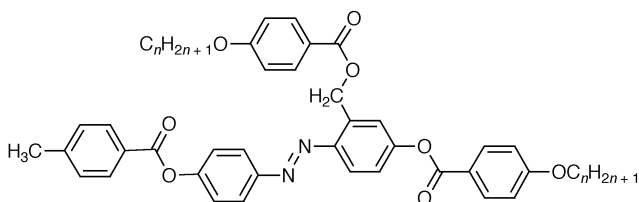
In this paper, we present the synthesis of two related series containing a 4-*n*-alkoxybenzoyloxy methylene lateral fragment (Scheme 3). These compounds have the same inner fragment, but differ by the number of aromatic rings in the main core: three in series I and four in series II. An additional advantage of these compounds is that flexible lateral substituents attached to a fairly long rigid core have the interesting ability



**Scheme 2**

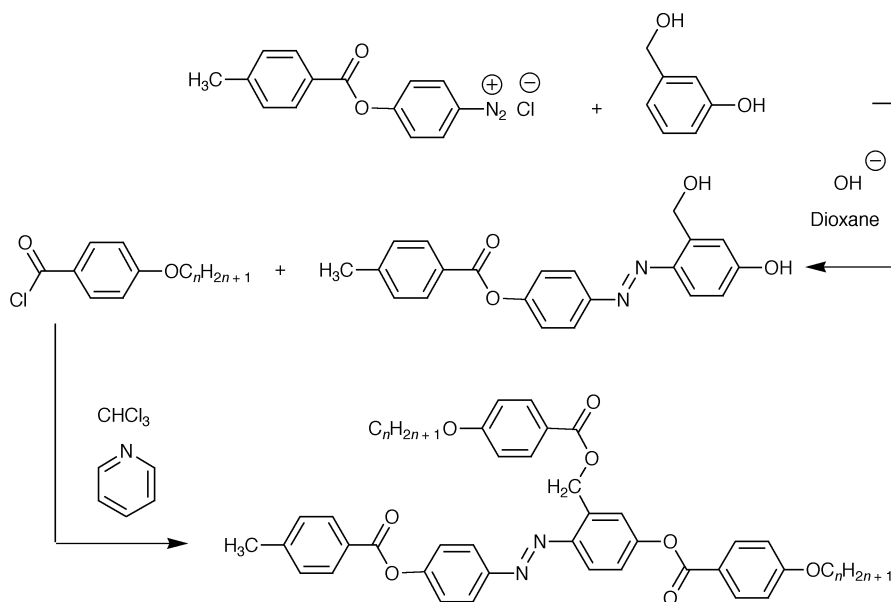


Series I: CO $n$ ,  $n = 2, 4, 6, 8, 10$



Series II: CO $Dn$ ,  $n = 4, 6, 8, 10, 12$

**Scheme 3**



COD $n$

**Scheme 4**

to decrease the melting temperatures while preserving the mesogenic properties.<sup>12–17</sup> We have investigated several types of lateral substituents: *N,N*-dialkylated amine, *N,N*-dialkylated methylene amine, alkoxy chains, a substituted benzoyloxy fragment and bifurcated alkoxy chains.<sup>10,13,16,17</sup> The comparison of the enforcement of the nematic properties among all these lateral substituents is of interest to understand the molecular packing in the nematic phase.

Thus, in this paper we will examine the following aspects of this problem: (1) the possibility for molecules having a 4-*n*-alkoxybenzoyloxy methylene fragment in the lateral chain to exhibit a liquid crystalline phase; (2) the thermal intramolecular cyclization of these compounds and the properties of the resulting nematic mixture; (3) some kinetic parameters of the reaction; and (4) the X-ray diffraction study of a related compound for structural determination.

## Experimental

### Synthesis

The synthetic scheme for series **II** is presented in Scheme 4 and the synthesis is briefly described in the following. In the first step, a solid *para*-substituted aniline hydrochloride used for the diazotization step was obtained through conventional methods.<sup>18</sup> The diazotization was then performed, using dioxane as solvent, by coupling the diazonium salt with 3-hydroxybenzyl alcohol under basic conditions.<sup>19</sup> The diazotization occurred mainly in the position *para* to the remaining hydroxyl group. After the evaporation of dioxane, the mixture was extracted with three portions of ether and washed three times with water. After drying and evaporating the solvent, the crude product was chromatographed on silica gel (60–200 mesh) with CH<sub>2</sub>Cl<sub>2</sub>–ethyl acetate (80 : 20), then eluted with CH<sub>2</sub>Cl<sub>2</sub>–methanol; the phenol was collected as the last fraction. Finally, this phenol was esterified with 4-*n*-alkoxybenzoyl chloride in a CHCl<sub>3</sub>–pyridine solvent. After acidification, the mixture was extracted with ether and washed two times with acidic water, two times with diluted ammonia and finally two times with water. After chromatography (silica gel 60–200 mesh, eluent CH<sub>2</sub>Cl<sub>2</sub>, first fraction), the final product was recrystallized in a mixture of toluene–ethanol–4-methylpentan-2-one (10 : 80 : 10) until constant transition points were obtained. The transition points were measured by DSC

**Table 1** Crystal data and structure refinement for compound **I4Cl**

Empirical formula	C <sub>28</sub> H <sub>20</sub> ClN <sub>2</sub> O <sub>4</sub>
Formula weight	483.91
Crystal system	Triclinic
Space group	<i>P</i> 1
Wavelength/Å	0.71073
Final <i>R</i> indices [ <i>I</i> > 2σ( <i>I</i> )]	<i>R</i> <sub>1</sub> = 0.041 <i>wR</i> <sub>2</sub> = 0.1143
<i>R</i> indices (all data)	<i>R</i> <sub>1</sub> = 0.055 <i>wR</i> <sub>2</sub> = 0.1253
<i>a</i> /Å	6.0244(6)
<i>b</i> /Å	12.731(2)
<i>c</i> /Å	15.0026(13)
α/°	75.052(8)
β/°	83.802(6)
γ/°	86.817(9)
<i>U</i> /Å <sup>3</sup>	1104.7(2)
<i>T</i> /K	173(2)
<i>Z</i>	2
Measured reflections	5835
Independent reflections	4511
<i>R</i> (int)	0.0220

(Mettler FP 52) using a heating rate of 15 °C min<sup>-1</sup>. All the compounds were fully characterized by <sup>1</sup>H and <sup>13</sup>C NMR, mass spectrometry using the electrospray method and elemental analysis [for example, **CO6** gave the following elemental analysis (calcd) in 1%: C: 74.3 (74.5), H: 7.56 (7.56), N: 3.96 (4.04) and **COD6** gave C: 72.8 (73.2), H: 6.51 (6.53), N: 3.59 (3.63)].

The compound used for the X-ray structure (labelled as **I4Cl**) was synthesized following the same scheme but using 1.1 equiv. of 4-chlorobenzoyl chloride in order to esterify only the phenol group. After chromatography [silica gel 60–200 mesh, eluent ethyl acetate–hexane (25 : 75), last fraction], the compound was heated in PEG 200 solvent at 250 °C for 20 min. The 2*H*-indazole compound was precipitated in water and then recrystallized in DMSO several times. The single crystal was grown from a DMSO solution by slow evaporation.

### NMR experiments

<sup>13</sup>C NMR experiments were performed using a Varian VXR-500 NMR spectrometer (*B*<sub>0</sub> = 11.07 T) equipped with an indirect detection probe manufactured by Narolac Cryogenic Corporation. The sample was put in a standard 5 mm tube and spun slowly (16 Hz) along the magnetic field so that the director in the liquid crystalline phase would align parallel to the magnetic field. To avoid RF overheating, a 0.8% decoupler duty cycle was used. Temperature calibration was made using pure ethylene glycol.

### X-Ray structure

The X-ray data were collected at –100 °C on a P4 Bruker-axs diffractometer using monochromated MoKα radiation (λ = 0.71073 Å). The data were corrected for Lorentz and polarization effects. An absorption correction was not applied since it was judged to be insignificant. The structure was solved by direct methods using SHELXTL (Bruker-axs) system and refined by full matrix least squares on *F*<sup>2</sup> using all reflections. Hydrogen atoms were included with idealized parameters. For 3763 observed reflections the final *R*<sub>1</sub> factor was 0.041. Details of the crystal data and refinement are given in Table 1.

CCDC reference number 440/153. See <http://www.rsc.org/suppdata/nj/1999/1223/> for crystallographic files in .cif format.

## Results and discussion

### Transition temperatures

The transition temperatures and the Δ*S*/*R* values of the five compounds synthesized in each series are given in Table 2.

For each compound, the two sets of values refer to the first heating cycle starting with the unmelted compound and the second heating cycle, respectively, with a heating rate of 15 °C min<sup>-1</sup>. The DSC curves of **COD12** obtained during the first and second cycling of the sample are presented in Fig. 1. Starting with the unmelted sample, two endothermic transitions are encountered, corresponding to a solid-solid transition and a solid-liquid transition. On a further increase in temperature, a broad exothermic peak corresponding to the cyclization reaction is observed and its maximum is located at 215 °C. After standing at 250 °C for 5 min, the sample was cooled down to room temperature. The nematic phase appears at 201 °C and persisted down to 117.5 °C. During the second heating, the nematic phase started at 143 °C and the exothermal peak is absent as the sample now contained a mixture of the 2*H*-indazole compound and 4-*n*-dodecyloxybenzoic acid. The DSC curve during the second cooling is very similar to the one obtained for the first cooling, indicating the sample did not undergo any further chemical changes with temperature. Further temperature cycling gave very similar thermograms. Therefore, we have obtained a nematic mixture of well-defined composition with reasonably reproducible transition temperatures.

After the cyclization, the <sup>1</sup>H NMR analysis of the mixture in CDCl<sub>3</sub> clearly shows the disappearance of the signal belonging to the hydrogens of the lateral –OCH<sub>2</sub>– (4.2 ppm) and the appearance of new peaks corresponding to the ethylenic hydrogen of the heterocyclic ring (8.8 ppm) and the acidic hydrogen of the carboxylic acid (12.4 ppm). In addition, we have performed thermogravimetric analysis (TGA) on some compounds within the two series using a dynamic method (airflow rate of 70 ml per min and a temperature ramp of 2 °C

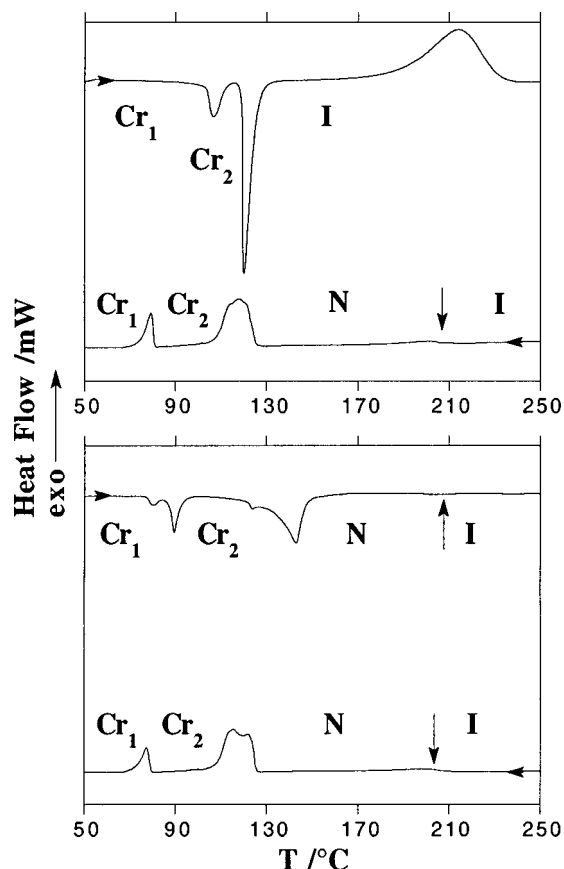


**Fig. 1** DSC curves of **COD12** during the first and the second thermal cycle (heating rate and cooling rate ±15 °C min<sup>-1</sup>). The vertical arrows give the position of the transition between the nematic and isotropic phase.

**Table 2** Transition temperatures (in °C) and  $\Delta S/R$  for series I and II

	Cycle	Cr <sub>1</sub>	→	Cr <sub>2</sub>	→	N	→	I <sub>1</sub>	→	I <sub>2</sub>
<b>Series I</b>										
<b>CO2</b>	1st	·	64	·	88.5	·	203	·		
	$\Delta S/R$		2.7		11.9		-27.5			
	2nd	·	98.5	·	152.5	·	163	·		
	$\Delta S/R$		3.9		6.5		0.70			
<b>CO4</b>	1st	·	76.5	·		·	203.5	·		
	$\Delta S/R$		16.9				-30.3			
	2nd	·	90.5	·	114	·	157	·		
	$\Delta S/R$		4.6		2.0		0.97			
<b>CO6</b>	1st	·	68	·	80	·	204.5	·		
	$\Delta S/R$		3.0		10.3		-27.7			
	2nd	·	86.5	·	104	·	153	·		
	$\Delta S/R$		4.5		2.5		0.76			
<b>CO8</b>	1st	·	71	·		·	205.5	·		
	$\Delta S/R$		27.7				-29.9			
	2nd	·	92.5	·	119	·	150	·		
	$\Delta S/R$		5.9		6.7		1.06			
<b>CO10</b>	1st	·	66.5	·		·	207	·		
	$\Delta S/R$		29.7				-29.9			
	2nd	·	94	·	111	·	147	·		
	$\Delta S/R$		8.8		11.5		0.26			
<b>Series II</b>										
<b>COD4</b>	1st	·	155	·			174*	·	208	·
	$\Delta S/R$		12.8						-29.0	
	2nd	·	131.5	·	166.5	·	247	·		
	$\Delta S/R$		4.1		5.4		0.36			
<b>COD6</b>	1st	·	120.5	·		·	148	·	211	·
	$\Delta S/R$		16.8				0.18		-34.5	
	2nd	·	102.5	·	166.5	·	236	·		
	$\Delta S/R$		4.2		11.3		0.36			
<b>COD8</b>	1st	·	92	·	121.5	·	134	·	212.5	·
	$\Delta S/R$		3.8		11.3		0.21		-27.7	
	2nd	·	100	·	181.5	·	223	·		
	$\Delta S/R$		3.7		9.4		0.22			
<b>COD10</b>	1st	·	109.5	·	114.5	·	123*	·	213.5	·
	$\Delta S/R$		2.8		23.5				-30.7	
	2nd	·	93.5	·	159.5	·	213	·		
	$\Delta S/R$		3.1		9.4		0.35			
<b>COD12</b>	1st	·	106.5	·	120	·	214.5	·		
	$\Delta S/R$		5.6		21.0		-27.7			
	2nd	·	89.5	·	142.5	·	206	·		
	$\Delta S/R$		4.0		14.9		0.26			

These values were taken with increasing temperature during the first (1st) and second (2nd) heating cycles (heating rate + 15 °C min<sup>-1</sup>). Cr, N, I<sub>1</sub> and I<sub>2</sub> refer to the solid phase, the nematic phase, the isotropic liquid before cyclization and the isotropic liquid after cyclization, respectively. The · indicates the observed phases and \* denotes a transition temperature observed by microscope at the same heating rate.

per min), which shows that during the cyclization the loss of mass is negligible.

Fig. 2 gives the thermal behavior of series I and II during the first heating step and the first temperature transition in the cooling step. For series II, a monotropic mesophase with a short nematic range was observed for the first four members of the series. This nematic phase is not observed for series I, whose core contains only three rings. In our previous study, we showed that the short CH<sub>2</sub> spacer permits the alignment of the lateral motif along the core.<sup>10</sup> The rigidity of the core, particularly the section of the core where the lateral substituent is hooked, is very important for inducing liquid crystal behavior. The choice of lateral substituent is also important. From the present and our previous works, we propose the following trend for the efficiency of these lateral fragments in promoting nematic properties: -CH<sub>2</sub>-N(R)<sub>2</sub> < -CH<sub>2</sub>-O-CO-phi-OR < -O-CH(R)<sub>2</sub> < -O-CH<sub>2</sub>-phi-A < -OR (where phi is a benzene ring, A is a substituent, R is a chain).

In Fig. 2, it is clear that the maximum of the cyclization peak is at the same temperature regardless of the chain length. This indicates, as expected, that the intramolecular reaction does not involve other parts of the molecule. In addition, unlike the other peaks on the DSC curve, the position of this peak is dependent on the temperature ramp. A slower ramp shifts this peak towards lower temperature, showing the effect

of thermal activation on the intramolecular reaction. The  $T_{IN}$  of the mixture depends on the number of rings in the 2*H*-indazole compound: from series I to series II, an average increase of 70 °C was observed.

In Fig. 3, we present the DSC curves of a homologous compound of series I in which the leaving molecule is H<sub>2</sub>O. During the cyclization, water is formed and leaves the medium at the reaction temperature, yielding the 2*H*-indazole compound, rather than a mixture. By comparing the transition temperatures between the reaction product and the pure 2*H*-indazole, we can have some idea about the cleanliness of the reaction. There is only a 10 °C decrease in the  $T_{IN}$  temperature between the two DSC curves, showing that the yield of the reaction is quite high and without significant amounts of byproducts.

### <sup>13</sup>C Chemical shift analysis

We chose to study by <sup>13</sup>C NMR the COD12 compound, because it does not have any enantiotropic nematic phase and its  $T_{KN}$  temperature is rather low. Prior to doing the NMR experiment, the sample was melted in an oven and then kept at 123 °C for 5 min. Fig. 4 presents the spectra of the sample at constant temperature ( $T = 123$  °C) as a function of time. The compound started in the isotropic phase. As the reaction

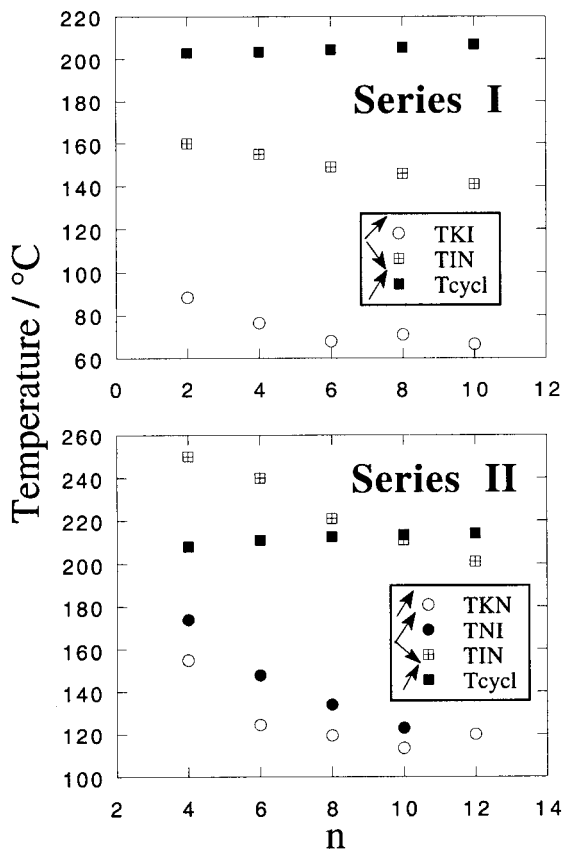


**Fig. 2** Thermal behavior of series I and II during the first heating step and the beginning of the first cooling step. The arrows indicate the heating or the cooling step.  $T_{\text{cycl}}$  is the position of the exothermic peak due to cyclization and the others are phase transition temperatures (for example,  $T_{\text{IN}}$  is the temperature at which the mixture starts to be nematic on cooling).

proceeded, some indazole molecules were formed, and this induced the transition of the melt into a nematic phase. At  $t = 75$  min (spectrum *c*), there was a coexistence of the isotropic and the nematic phases. After this, the mixture was purely nematic and the sample was quite homogeneous, as indicated by the reasonable linewidths of the peaks obtained in the nematic phase.

The aromatic peaks (above 100 ppm) show large positive jumps because of chemical shift anisotropies caused by the alignment of the molecules, which have a positive anisotropy of the magnetic susceptibility ( $\Delta\chi$ ) due to the aromatic rings in the core. The aliphatic peaks (below 80 ppm) seem to have negative jumps in the nematic phase, especially those of the  $-\text{CH}_2\text{O}-$  groups. However, a careful analysis must be made to assign the peaks. In the isotropic phase, the two  $-\text{CH}_2\text{O}-$  groups in the dodecyloxy chains have nearly the same chemical shift in the isotropic liquid (*i.e.*, 68.71 and 68.57 ppm), while the lateral  $-\text{CH}_2\text{O}-$  group is more shielded (62.28 ppm). The corresponding assignment is given in Fig. 4. In the nematic phase, the two  $-\text{CH}_2\text{O}-$  groups in the dodecyloxy chains would experience negative jumps like the other carbons in these chains, but the magnitude of the jumps would not be the same because of different orientations of the chains. The one attached to the central core would experience a larger negative jump and the one attached on the lateral phenyl ring would have a smaller negative jump due to the particular orientation of the lateral fragment.<sup>12</sup> Conversely, the orientation of the  $-\text{CH}_2\text{O}-$  group directly attached to the core would cause this fragment to have a positive jump, as observed in similar compounds.<sup>10</sup> These considerations led to the assignment given in Fig. 4(*d*).

With increasing time, three major features can be noted: (1) the sample seemed to be homogeneous, because the linewidths

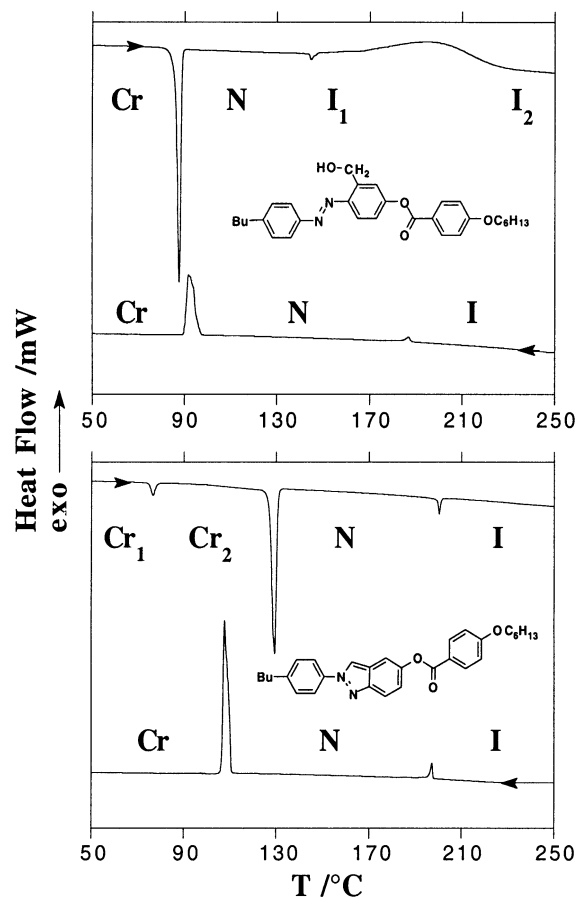
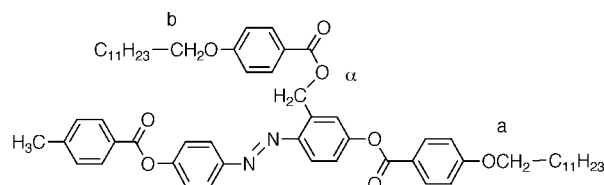


**Fig. 3** DSC curves of a parent compound of CO6, in which the lateral chain contains the  $-\text{CH}_2\text{OH}$  motif, and of the pure cyclized compound during the first cycle of heating and cooling (heating rate and cooling rate  $\pm 15^\circ\text{C min}^{-1}$ ).

were quite constant with time; (2) the ordering of the phase gradually increased, as indicated by the increase of the aromatic carbon chemical shifts; and (3) the rate of the internal cyclization is rather slow at this temperature as no extra peak is clearly seen in the aromatic region after 4 h. In the  $-\text{CH}_2\text{O}-$  region, there is accordingly no obvious disappearance of the  $-\text{CH}_2\text{O}-$  signal associated with the lateral group attached to the core. Therefore, we conclude that, when the mixture started to be nematic, only a small percentage of molecules had reacted. This small amount was sufficient to orient the remaining unreacted COD12 compound.

#### Activation energy

The activation energy of the cyclization process was simply determined by observing the reaction under the polarizing microscope in the following way. If we assume that at any temperature the nematic phase starts to form when a fixed concentration of the 2*H*-indazole compound is produced, we can follow the kinetics of the reaction by tracking the time  $t_{\text{app}}$  for the first liquid crystal droplet to appear in the melt, at each temperature. If we further assume that the cyclization of the compound obeys first-order kinetics, an Arrhenius dependence of the kinetic constant gives:  $\ln(t_{\text{app}}) = A + E_a/RT$ . In Fig. 5, the kinetic curves for all the compounds of the two series are presented. For compounds in series I, we have



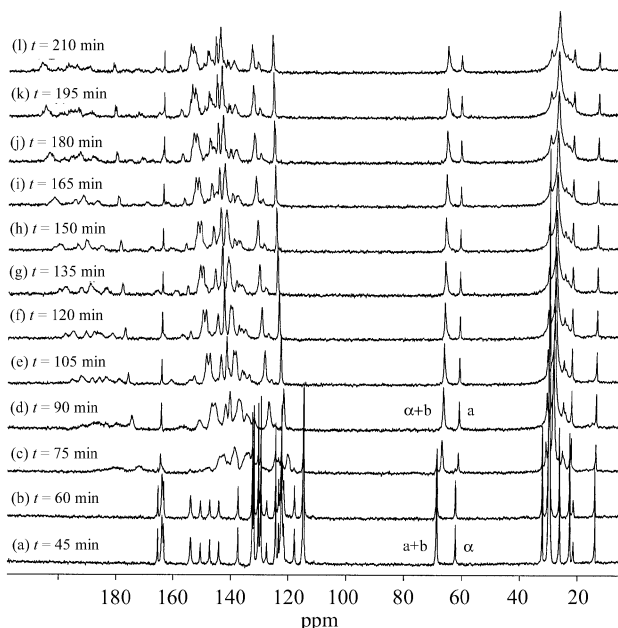


**Fig. 4**  $^{13}\text{C}$  NMR spectra of **COD12** compound at  $123^\circ\text{C}$  with increasing time. For each spectrum, the number of scans is 200, acquisition time 0.09 s, recycle delay 1.9 s, with a decoupler power of 17 kHz.

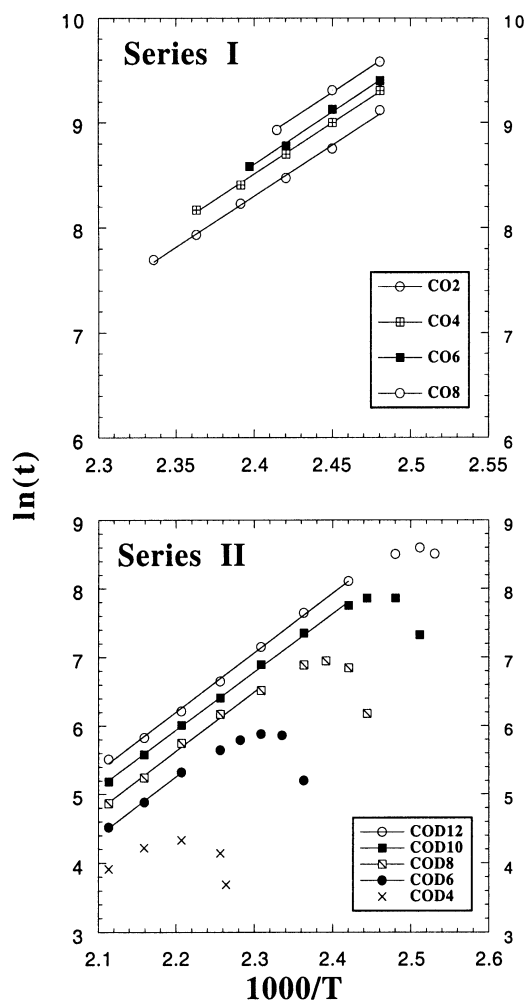


**Fig. 5** Plot of  $\ln(t_{\text{app}})$  as a function of  $1000/T$  for series I and II,  $t_{\text{app}}$  being the time when the first nematic droplet appears in the melt of the sample at constant temperature. The last temperature was taken to be  $2^\circ\text{C}$  in series II ( $5^\circ\text{C}$  in series I) above the clearing temperature of the first run for **COD4**, **COD6**, **COD8**, **COD10** and  $2^\circ\text{C}$  above the melting temperature for **COD12**.

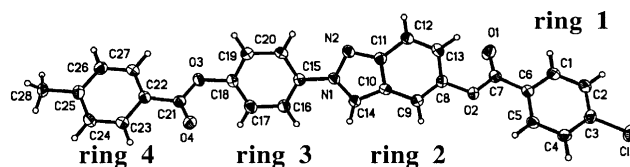


**Fig. 6** X-ray ball-and-stick structure, showing the atomic numbering, of **14Cl** at  $T = -100^\circ\text{C}$ .

explored temperatures between  $5^\circ\text{C}$  below the clearing temperatures and down to  $130^\circ\text{C}$ . In this range of inverse temperatures, a linear behavior is obtained. The curves are almost parallel, which is reasonable because the activation energy would not be dependent on the chain lengths. From the slope, an activation energy of  $E_a = 81.8 \pm 1.2 \text{ kJ mol}^{-1}$  was obtained. For compounds in series II, a linear behavior is observed for temperatures considerably below the melting point. From the mean slope of the linear segments for the last four members of the series, the activation energy was found to be  $E_a = 71.5 \pm 0.8 \text{ kJ mol}^{-1}$ . The difference between the activation energies reflects the difference in the nucleophilicity of the nitrogen N1 in both series. In series II, the oxygen in the *para* position enforces the electron density in the aromatic ring and consequently on nitrogen N1 as well; this effect is far less important with the butyl chain in series I. Near the melting point in series II, it took less time for the first nematic droplet to appear, and the curve is no longer linear. This indicates that the starting material will help the formation of the nematic phase despite the fact that it is itself in an isotropic phase to start with. As expected, the curvature near the melting temperature is more prominent if the nematic phase exists (compare **COD12** to the other compounds).

#### Structure analysis

It was not possible to grow single crystals of the indazole compounds containing a terminal alkoxy chain. Therefore, we present the X-ray structure of a compound (labelled as **14Cl**) having the same core containing the *2H*-indazole ring, but differing in the end group: a terminal chlorine is introduced instead of the terminal alkoxy chain.

As shown in Fig. 6, the three phenyl rings are designated as ring 1 (atoms C1 to C6), ring 3 (atoms C15 to C20), and ring 4 (atoms C22 to C27). The fused indazole unit is perfectly planar, and is designated as ring 2 (atoms C8 to C14). The global geometry of the molecule can be defined by the angles between the planes of the different rigid fragments as follows:  $\angle \text{plane}(\text{ring1})\text{-plane}[\text{C6-C7-(O1)-O2}] = 12.19^\circ$ ,  $\angle \text{plane}$ -

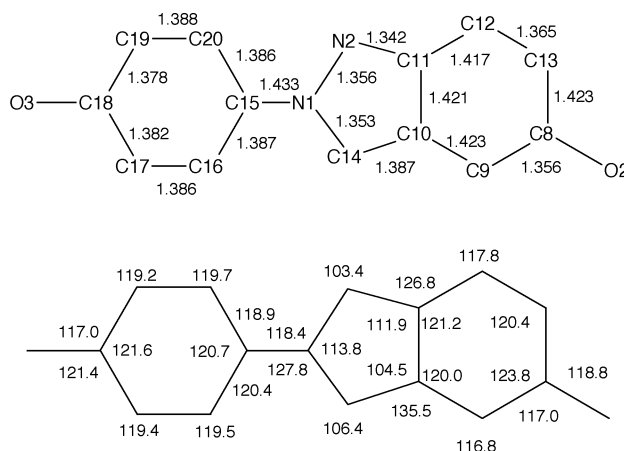


**Fig. 7** Bond lengths ( $\text{\AA}$ ) and angles ( $^\circ$ ) of the central section of **14Cl**.

**Table 3** Selected torsion angles (in deg) deviating significantly from the plane

C8–O2–C7–O1	– 6.57(0.27)	C8–O2–C7–C6	173.23(0.15)
C5–C6–C7–O1	–167.82(0.19)	C1–C6–C7–O1	11.74(0.28)
C5–C6–C7–O2	12.39(0.24)	C1–C6–C7–O2	–168.05(0.16)
C7–O2–C8–C9	133.93(0.18)	C7–O2–C8–C13	–52.63(0.22)
O2–C8–C9–C10	173.89(0.15)	O2–C8–C13–C12	–174.17(0.16)
C21–O3–C18–C19	–122.43(0.18)	C21–O3–C18–C17	60.88(0.23)
O4–C21–C22–C27	165.70 (0.18)	O3–C21–C22–C27	–15.01(0.24)
O4–C21–C22–C23	–14.72(0.27)	O3–C21–C22–C23	164.57(0.16)

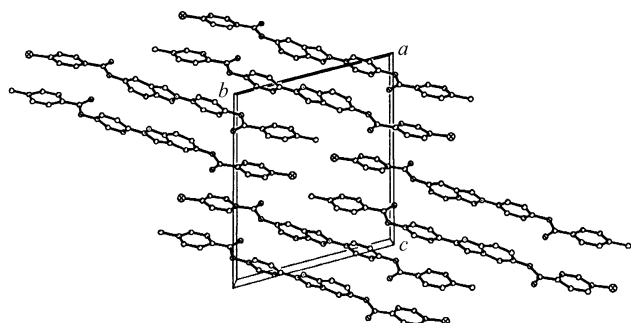
$[\text{C6–C7–(O1)–O2}]$ –plane(ring2) = 1.05°,  $\angle$  plane(ring2)–plane(ring3) = 1.25°,  $\angle$  plane(ring3)–plane[C22–C21–(O4)–O3] = 58.85° and  $\angle$  plane[C22–C21–(O4)–O3]–plane(ring4) = 14.99°. It can be seen that rings 2 and 3 are nearly parallel, indicating the extended  $\pi$ -electron delocalization between these two rings induced by the N1 lone pair. Due to this conjugation, this nitrogen is  $\text{sp}^2$  hybridized.

Fig. 7 gives the bond lengths and bond angles in the central section of the molecule. The central heterocyclic core is usually considered as a delocalized aromatic system rather than as dienes with localized bonding.<sup>6</sup> However, the bond lengths in the six-membered ring of the indazole reflect different bond orders for the C–C bonds: the C8–C13, C11–C12, C10–C11 and C9–C10 bonds are longer than the C12–C13 and C8–C9 bonds. Due to the coplanarity of the fused ring 2 system and ring 3, there is a strong repulsion between H14 and H16, causing a significant opening of the C14–N1–C15 angle. The central core is slightly bent due to the non-coplanarity of the N1–C15 and C8–O2 bonds at each side of the indazole structure. The angle between these two bonds is equal to 157°, which is very near the value of 155° measured in a related compound.<sup>20</sup>

The molecular conformation is entirely defined by the torsion angles deviating by more than 10° from coplanarity (Table 3). As expected, these angles involve the two carboxylate fragments, which are not in the same plane as the rings.

To keep the global rod-like shape of the molecules, the two carboxylate groups point in opposite directions and the long molecular axis is nearly aligned with the *para* axis of ring 3. The  $C_2$  axis of ring 1 is relatively off from this direction.

The projection of the crystal structure along the *a* axis is presented in Fig. 8. The long axes of the molecules are quasi-parallel; the molecules are perfectly parallel to each other because of crystallographic center of symmetry ( $P\bar{1}$  space group). The molecules are aligned along a unique direction, having an arrangement typical of a nematogen compound. They have the appearance of forming end-to-tail pairs. However, the interactions between neighboring molecules are very weak, and the shortest interatomic distances are very close to the sum of van der Waals radii. For example, the distance between C11 and C28 of pair molecules is 3.593 Å and the distance between two chlorine atoms of adjacent molecules is 3.705 Å.

**Fig. 8** Projection of the crystal cell along the *a* axis for **14Cl**.

## Conclusion

We have synthesized two new series of compounds containing an active methylene in the *ortho* position of the diazo link in a diphenyl diazene moiety. One series contains three phenyl rings and the second one contains four; both series contain a lateral 4-*n*-alkoxybenzoyloxymethylene group. In spite of the presence of this bulky fragment in the lateral chain, an enantiotropic nematic phase is present when the core contains four rings. Compounds in both series underwent an internal cyclization between 200 and 215°C, forming nematic mixtures composed of a nematogenic 2*H*-indazole derivative and 4-*n*-alkoxybenzoic acid. The mixtures obtained exhibit large nematic ranges, which persist over further cooling-heating cycles. <sup>13</sup>C NMR indicates that at constant temperature the mixture starts to become nematic even when the extent of the intramolecular reaction is quite small. This can be attributed to the anisotropic shape of the starting molecule, such that the formation of only a few percent of mesogenic molecules force the entire sample to change into a liquid crystalline state. This result permits us to extract the activation energy from the time it takes the first liquid crystalline droplet to appear in the mixture at a constant temperature. The activation energy of cyclization was found to be 81.8 ± 1.2 and 71.5 ± 0.8 kJ mol<sup>-1</sup> for the series having three rings and four rings in the main core, respectively. The X-ray structure of a parent compound containing the 2*H*-indazole fragment indicates that the indazole ring and the directly attached aromatic rings are nearly in the same plane, indicating an extended  $\pi$ -electron delocalization between these two rings induced by the N lone pair. The angle between the two bonds at each side of the 2*H*-indazole ring is equal to 157°. Therefore, the 2*H*-indazole fragment can act as an interesting rigid structure to build new slightly bent mesogenic molecules.

## Acknowledgements

The work of BMF was supported by the U.S. National Science Foundation under grant number DMR-9700680.

## References

- 1 M. P. Cava, I. Noguchi and K. T. Buck, *J. Org. Chem.*, 1973, **38**, 2394.
- 2 R. Fusco, A. Marchesini and F. Sannicolo, *J. Heterocyclic Chem.*, 1987, **24**, 773.
- 3 R. Bartsch and I.-W. Yang, *J. Heterocyclic Chem.*, 1984, **21**, 1063.
- 4 L. Chardonens and M. Buchs, *Helv. Chim. Acta*, 1940, **23**, 1399.
- 5 L. Chardonens and P. Heinrich, *Helv. Chim. Acta*, 1946, **29**, 872.
- 6 L. C. Behr, in *Heterocyclic Compounds*, ed. R. H. Wiley, Wiley-Interscience, New York, 1967, vol. 22, pp. 289.
- 7 P. Freundler, *Bull. Soc. Chim. (Paris)*, 1903, **29**, 742.
- 8 P. Freundler, *Bull. Soc. Chim. (Paris)*, 1904, **31**, 863.
- 9 P. Freundler, *Bull. Soc. Chim. (Paris)*, 1904, **31**, 868.

- 10 C. Canlet, P. Judeinstein, J.-P. Bayle, F. Roussel and B. M. Fung, *Liq. Crystals*, 1999, **26**, 281.
- 11 G. W. Gray and B. Jones, *J. Chem. Soc.*, 1953, 4179.
- 12 F. Perez, J.-P. Bayle and B. M. Fung, *New J. Chem.*, 1996, **20**, 537.
- 13 F. Perez, P. Judeinstein, J.-P. Bayle, F. Roussel and B. M. Fung, *Liq. Crystals*, 1997, **22**, 711.
- 14 A. Jacobi and W. Weissflog, *Liq. Crystals*, 1997, **22**, 107.
- 15 V. S. Bezborodov and V. F. Petrov, *Liq. Crystals*, 1997, **23**, 771.
- 16 F. Perez, P. Judeinstein, J.-P. Bayle, H. Allouchi, M. Cotrait, F. Roussel and B. M. Fung, *Liq. Crystals*, 1998, **24**, 627.
- 17 C. Canlet, P. Judeinstein, J.-P. Bayle, F. Roussel and B. M. Fung, *New J. Chem.*, 1998, **22**, 211.
- 18 A. Nose and T. Kudo, *Chem. Pharm. Bull.*, 1981, **29**, 1159.
- 19 F. Perez, P. Judeinstein and J.-P. Bayle, *New J. Chem.*, 1995, **19**, 1015.
- 20 S. Nan'ya, K. Katsuraya, E. Maekawa, K. Kondo and S. Eguchi, *J. Heterocyclic Chem.*, 1987, **24**, 971.

Paper 9/07124E